

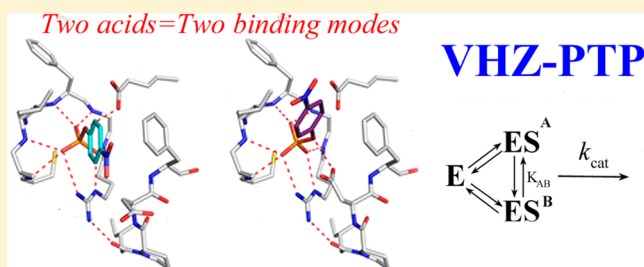
New Functional Aspects of the Atypical Protein Tyrosine Phosphatase VHZ

Vyacheslav I. Kuznetsov and Alvan C. Hengge*

Department of Chemistry and Biochemistry, Utah State University, Logan, Utah 84322-0300, United States

Supporting Information

ABSTRACT: LDP3 (VHZ) is the smallest classical protein tyrosine phosphatase (PTP) known to date and was originally misclassified as an atypical dual-specificity phosphatase. Kinetic isotope effects with steady-state and pre-steady-state kinetics of VHZ and mutants with *p*-nitrophenol phosphate have revealed several unusual properties. VHZ is significantly more active than previously reported but remains one of the least active PTPs. Highly unusual for a PTP, VHZ possesses two acidic residues (E134 and D65) in the active site. D65 occupies the position corresponding to the typical general acid in the PTP family. However, VHZ primarily utilizes E134 as the general acid, with D65 taking over this role when E134 is mutated. This unusual behavior is facilitated by two coexisting, but unequally populated, substrate binding modes. Unlike most classical PTPs, VHZ exhibits phosphotransferase activity. Despite the presence of the Q-loop that normally prevents alcoholysis of the phosphoenzyme intermediate in other classical PTPs, VHZ readily phosphorylates ethylene glycol. Although mutations of Q-loop residues affect this phosphotransferase activity, mutations on the IPD loop that contains the general acid exert more control over this process. A single P68V substitution on this loop completely abolishes phosphotransferase activity. The ability of native VHZ to catalyze transphosphorylation may lead to an imbalance of intracellular phosphorylation, which could explain the correlation of its overexpression with several types of cancer.



The protein tyrosine phosphatases (PTPs) are a large family of enzymes responsible for intracellular dephosphorylation. Together with protein tyrosine kinases (PTKs), PTPs control the level of protein phosphorylation, which modulates numerous aspects of cell life, such as growth, proliferation, metabolism, intercellular interaction, immune responses, and gene transcription.¹ PTPs contain a highly conserved HCXXGXXRS/T signature sequence motif but share very few sequence similarities outside of the conserved regions, which are comprised of the phosphate binding loop (P-loop); the general acid loop, often termed the WPD loop; and the Q-loop that bears conserved glutamine residues that orient the water nucleophile in classical PTPs and prevent phosphotransferase activity to other potential nucleophiles.

All PTPs utilize a two-step double-displacement mechanism of phosphate monoester hydrolysis (Scheme 1) mediated by an invariant cysteine-arginine-aspartic acid triad of catalytic residues.² The mechanism proceeds through a phosphoenzyme intermediate in which the second chemical step is often rate-limiting.³ In the first step, the P-loop orients the substrate as the nucleophilic cysteine attacks phosphorus with simultaneous expulsion of the leaving group protonated by the catalytic general acid. In the second step, a water molecule, directed by the aspartic acid residue that served as the general acid in the first step and Q-loop glutamine residues, attacks the phosphoenzyme intermediate.

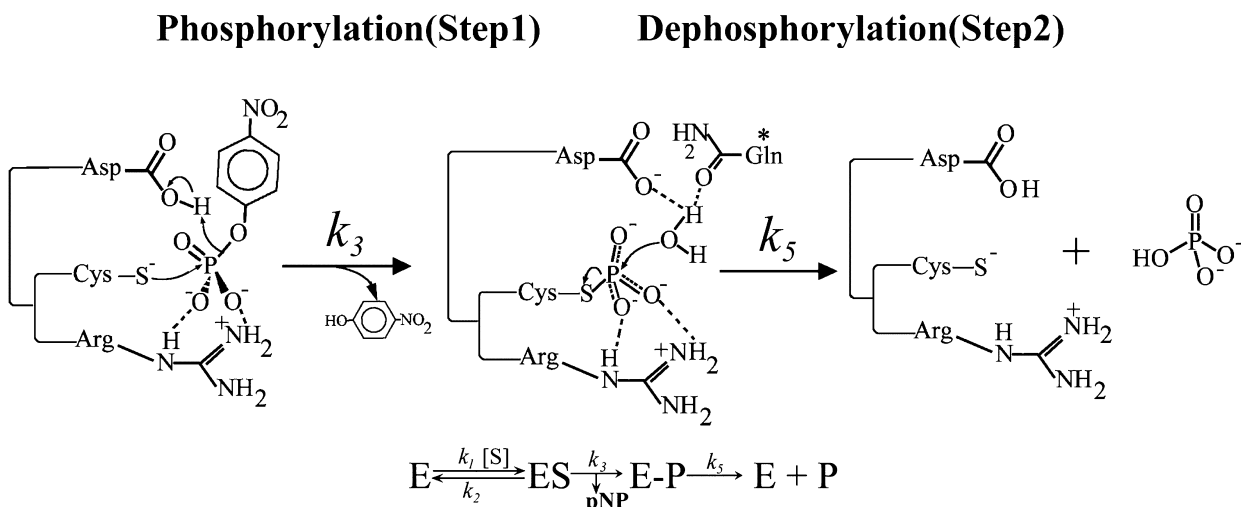
The PTP family is subdivided into several groups based on substrate specificity, subcellular localization, and size. Members

of the classical PTP family selectively hydrolyze phosphotyrosine-containing peptides, and this family includes the well-studied bacterial effector protein YopH, responsible for the virulence of notorious *Yersinia pestis*, and human PTP1B, which plays an important role in insulin signaling.⁴ Classical PTPs have a modular organization and, in addition to the catalytic phosphatase domain, contain noncatalytic domains that control subcellular localization and protein–substrate interactions. All classical PTPs are tyrosine specific enzymes. Members of the dual-specificity phosphatase (DSP) subfamily hydrolyze phosphoserine and phosphothreonine in addition to phosphotyrosine-containing target sites. Within the DSP subfamily, the atypical DSPs are smaller and contain only a catalytic domain.⁵ The classical PTPs and DSPs also differ in their phosphotransferase ability. In classical PTPs, the phosphoenzyme intermediate is attacked only by water because of the shielding effect of conserved Q-loop residues, named for the presence of conserved glutamines.⁶ In contrast, DSPs such as VHR and the low-molecular weight (LMW) Ltp1, both of which lack the Q-loop, display significant phosphotransferase ability.⁷ On this basis, it has been concluded that the presence of the Q-loop prevents phosphotransferase activity.

Received: June 17, 2013

Revised: September 16, 2013

Published: September 27, 2013

Scheme 1. Chemical Steps in the Reaction Catalyzed by PTPs^a

^aIn the first chemical step, a nucleophilic cysteine attacks the phosphate ester with simultaneous protonation of the leaving group by the conserved aspartic acid. In the second chemical step, water attacks the phosphoenzyme intermediate liberating inorganic phosphate and free enzyme. Forward rate constants are numbered with odd subscripts, and reverse rate constants are numbered with even subscripts. The Q-loop that is present only in classical PTPs serves to orient the incoming nucleophilic water and most commonly contains a catalytic glutamine residue marked with an asterisk. This residue is represented by isosteric glutamic acid E134 in VHZ.

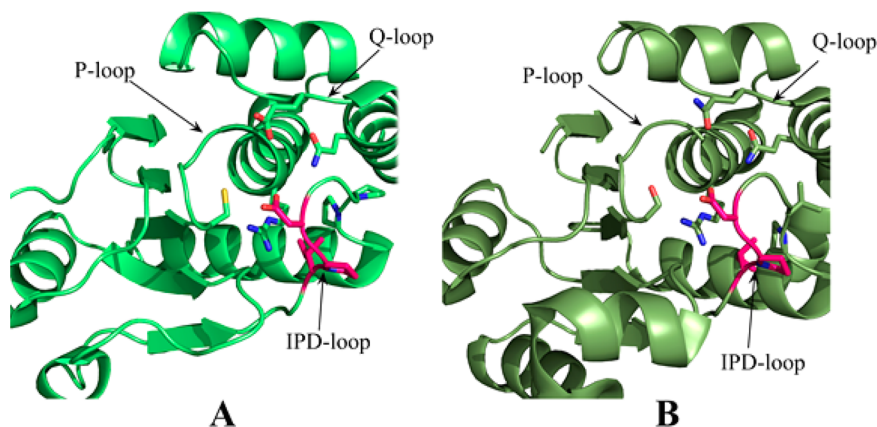


Figure 1. Side-by-side comparison of (A) VHZ/PTP (PDB entry 4ERC) and (B) SsoPTP (PDB entry 2I6J). The proteins are very similar in size and structure, and both contain a rigid IPD loop (colored red) in contrast to the conserved WPD loop in classical PTPs. Both proteins lack an N-terminal substrate recognition loop and contain no additional extracatalytic domains.

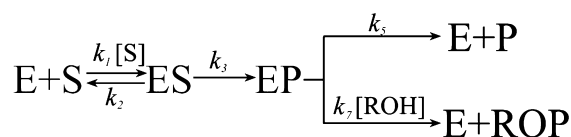
VHZ, and the closely related phosphatase *Sulfolobus solfataricus* PTP (SsoPTP), are among the smallest classical PTPs known to date (Figure 1). The SsoPTP (161 amino acids) is similar to VHZ (150 amino acids) in size and catalytic activity. Both VHZ and SsoPTP consist of a single, catalytic domain that is more similar to classical PTPs than DSPs^{8,9} and contain identical secondary structural elements but, unlike most classical PTPs, lack an N-terminal extension that forms a substrate recognition/binding loop. Like VHZ, the general acid in SsoPTP resides on a rigid IPD loop, which, unlike the flexible WPD loop in classical PTPs, permanently occupies a closed conformation. Unlike VHZ, and like classical PTPs, SsoPTP/WT contains no additional general acid in its Q-loop region. VHZ was originally classified as an atypical DSP and named after its prototypical member as VH1-related protein member Z. In previous work, we presented results indicating that VHZ should be classified as a PTP rather than a DSP, on the basis of a structural analysis and results of a phosphopeptide

substrate screen in which VHZ showed activity against pY-containing peptides but not toward pS or pT peptides.⁸

In this work, we show that the catalytic activity of VHZ was significantly underestimated in previous reports, as a result of pronounced product inhibition, and the inhibitory effect of certain buffers. Despite having much in common with classical PTPs, VHZ is highly unusual in possessing two acidic residues in the active site, D65 and E134. Our results indicate that under certain circumstances either of these residues can serve as the general acid in the first step of the reaction. We also present results demonstrating that VHZ, despite the presence of a Q-loop, catalyzes the transfer of a phosphoryl group to alcohols (alcoholysis) in addition to water (hydrolysis) (Scheme 2).

The mutagenesis of several residues in VHZ in parallel with SsoPTP has revealed that, in addition to the Q-loop, particular residues in the general acid IPD loop play a crucial role in nucleophilic selectivity. A combination of kinetics and mutagenesis experiments have revealed unusual aspects of the kinetic behavior of VHZ and provided insights into factors that control

Scheme 2. Partitioning of the Enzyme–Phosphate Intermediate between Hydrolysis and Alcoholysis Pathways^a



^aAlcohols, or a water nucleophile, in two competing pathways attack the phosphoenzyme intermediate formed in the first step.

the phosphotransferase activity of VHZ, and possibly in other PTPs.

■ EXPERIMENTAL PROCEDURES

Protein Cloning, Expression, and Purification. VHZ mutants were created using the Qiagen QuikChange Lightning Site-Directed Mutagenesis Kit. VHZ and mutants were purified as previously described.⁸ A His-tagged version of VHR was prepared as follows. In the first step, the gene of VHR was amplified from the pT7-7 plasmid using Fwd1 (**GAAAACCTGTATTTTCAGGGCATGTCGGGCTCGTTCGAGCT**) and Rev1 (**GGAGAGCTCCTAGGGTTCAACTTCCCCTCCTTGCTAG**) to incorporate the TEV protease cleavage site (Fwd1, bold) immediately upstream of the protein gene and the SacI restriction site (Rev1, bold) added at the end of the gene sequence. In the second step, the product of the first polymerase chain reaction (PCR) step was used as a template and a KpnI restriction site was added upstream of the TEV protease cleavage sequence using primers Fwd2 (**CGGGT-ACCGAAAACCTGTAT**) and Rev1 (**GGAGAGCTCCTAGGGTTCAACTTCCCCTCCTTGCT**). The resulting PCR product was digested with KpnI and SacI (Fermentas) and ligated into the pet-45(B+) vector (Novagen) predigested with the same set of restriction enzymes. The *Escherichia coli* DH5 α competent cells were transformed with 5 μ L of the ligation mixture and plated on an ampicillin-containing agar plate. DNA sequencing confirmed the presence of the desired gene. BL-21 DE-3 (codon+) *E. coli* competent cells were transformed with the pet-45(B+)-VHR vector. Ten milliliters of Luria-Bertani medium was inoculated with a single colony and incubated at 37 °C on a shaker overnight; 1 L of 2 \times YT medium containing ampicillin and chloramphenicol was inoculated with 10 mL of overnight cell growth. The cells were grown at 37 °C until OD₆₀₀ reached 1.2–1.5; 100 mg of IPTG was added (final concentration of 100 mg/L), and the flask was transferred to a room-temperature shaker and incubated for 18–20 h. The cells were harvested by centrifugation and resuspended in Ni loading buffer containing 50 mM Tris, 500 mM NaCl, 20 mM imidazole, 5 mM 2-mercaptoethanol, and 5% glycerol (pH 8.0). Cells were sonicated on ice, and after centrifugation, the supernatant was decanted and filtered through a 0.45 μ m Millipore syringe filter. Ni-fast flow high-affinity resin (GE Healthcare) was washed three times with Ni loading buffer and incubated with the supernatant for 30 min at 4 °C while being gently shaken. The resin slurry was transferred to a 15 mL glass chromatography column. The column was extensively washed with Ni loading buffer to reach baseline absorbance, and protein was eluted with a 120 mL linear gradient with buffer containing 50 mM Tris, 500 mM NaCl, 20 mM imidazole, 2-mercaptoethanol, and 5% glycerol (pH 8.0) at a rate of 2 mL/min. The fusion VHR protein obtained was dialyzed stepwise in TEV cleavage buffers

containing 50 mM Tris base, 0.5 mM EDTA, 3 mM DTT, 5% glycerol, and a reducing concentration of NaCl (300, 150, or 0 mM), at a rate of 1.5 h/step followed by addition of 2 mg of TEV protease. The cleavage of VHR was rapid and complete in 2 h at 4 °C. VHR was dialyzed in the original Ni loading buffer to remove DTT and EDTA for 2 h, and the solution was passed through Ni-fast flow high-affinity resin to remove the cleaved polyhistidine tag and TEV protease. The collected supernatant was concentrated to 3–5 mL using a Millipore centrifuge concentrator tube and loaded on a Superdex 75 26/60 gel filtration column (GE-Healthcare) pre-equilibrated with buffer containing 50 mM HEPES, 150 mM NaCl, 50 mM imidazole, 5 mM DTT, and 10% glycerol. A single peak corresponding to the VHR was collected, concentrated to 6 mg/mL, flash-frozen in liquid nitrogen, and stored at –80 °C.

Cloning and Purification of SsoPTP. The *S. solfataricus* PTP gene sequence from Uniprot (entry Q97VZ7) was optimized for the *E. coli* expression system and synthesized by GenScript delivered in a shuttle vector. The gene was ordered with a KpnI restriction site followed by a TEV cleavage site directly upstream of the SsoPTP sequence and a SacI restriction site directly downstream of the stop codon. The shuttle vector containing the described gene was amplified in *E. coli* DH5 α , isolated, and digested with KpnI and SacI restriction enzymes in Green Buffer (Fermentas). The digestion products were separated by electrophoresis using a 1% agarose gel. The band that corresponded to the desired gene was extracted using the Qiagen Gel Extraction Kit and ligated into the pet45 (B+) plasmid predigested with the same set of restriction enzymes. Unfortunately, unlike VHR (and similar to VHZ⁸), the resulting fusion protein was resistant to TEV cleavage, so the poly-His tag and TEV cleavage site were removed from the pet45B(+)-SsoPTP vector by one-step overlapping PCR using primers: Fwd (TATACCATGTACTGGTCCGTCGAAAACG) and Rev (GACCCAGTACATGGTATATCTCCTTCTTAAAGTAAACAAAATTATTCTAG). Tagless SsoPTP was expressed in *E. coli* BL-21 DE-3 (codon+) cells. The growth and expression conditions were analogous to those used for VHZ and VHR. The cells were harvested by centrifugation and resuspended in the buffer containing 50 mM Tris, 1 mM EDTA, 10 mM DTT, and 5% glycerol (pH 7.4, 4 °C). Cells were disrupted by sonication on ice, and the pellet was separated by centrifugation. The supernatant was treated with a 10% (w/v) solution of polyethyleneimine (PEI, $M_w = 50000$, pH 8.0 and 4 °C) added dropwise at 4 °C to reach a final PEI concentration of 0.5% (w/v). After centrifugation, the supernatant was loaded at a rate of 1 mL/min on a Q-HiTrap (GE Healthcare) column pre-equilibrated with buffer containing 50 mM sodium acetate, 1 mM EDTA, and 3 mM DTT (pH 5.5). After being washed, the protein was eluted with a 120 mL linear gradient (2 mL/min) of buffer containing 50 mM sodium acetate, 1 mM EDTA, 600 mM NaCl, and 3 mM DTT (pH 5.5). A single isolated peak eluted at 200–250 mM NaCl corresponding to SsoPTP and was concentrated to 3–5 mL and loaded on a Superdex 75 26/60 gel filtration column (GE Healthcare) pre-equilibrated with buffer containing 25 mM Tris, 50 mM imidazole, 150 mM NaCl, 1 mM EDTA, and 5 mM DTT (pH 7.5 and 4 °C). A single peak was collected, concentrated to 10 mg/mL (A_{280} of a 1 mg/mL solution = 2.36), and flash-frozen in liquid nitrogen in the same buffer with 25% glycerol added.

YopH, PTP1B, and their mutants were expressed and purified as previously described.^{10,11}

All enzymes were purified to $\geq 99\%$ homogeneity based upon sodium dodecyl sulfate–polyacrylamide gel electrophoresis analysis (data not shown). The concentration of each enzyme was determined by measuring the absorbance at 280 nm using calculated extinction coefficients.

Preparation of *p*-Nitrophenyl Phosphate (*p*NPP). The dicyclohexylammonium salt of *p*NPP was synthesized as previously described.¹² A phosphate free solution of *p*NPP was prepared in two separate steps. The crude product was dissolved in a minimal volume of 0.8 M NaOH. Neutral cyclohexylamine was extracted with five equal portions of chloroform, accompanied by a reduction of the pH to 8.0–8.5. Inorganic phosphate was precipitated by addition of a solution containing 1 M MgCl and 5 M NH₄Cl (1:5 Mg²⁺:NH₄⁺ ratio) to yield a final magnesium concentration of 0.1 M. The pH was adjusted to 9.0–9.3 with ammonium hydroxide and the mixture stirred for 10 min until the solution turned cloudy because of the precipitation of MgNH₄PO₄. The concentration of *p*NPP in solution remains essentially unchanged, in contrast to calcium or magnesium chloride precipitation alone, which mostly precipitates *p*NPP. The precipitate was removed by filtration using a fritted glass funnel, and 10 g of a preactivated Chelex 100 resin suspension in water (pH 9.0) was added to scavenge the remaining magnesium. The resin was removed by filtration, and a cyclohexylammonium hydrochloride (Fisher) solution (pH 8–9) was added. The dicyclohexylammonium salt of *p*NPP precipitated and was collected by filtration, washed with cold absolute ethanol, and dried overnight under vacuum to yield the phosphate free dicyclohexylammonium salt of *p*NPP as a white solid, which was stored at $-20\text{ }^{\circ}\text{C}$ under nitrogen.

The sodium salt of *p*NPP allows the preparation of higher-concentration stock solutions and was produced by dissolving the dicyclohexylammonium salt, obtained as described above, in a 0.8 M NaOH solution followed by removal of cyclohexylamine by chloroform extractions. The pH of the aqueous layer was adjusted to pH 12 with 0.1 M NaOH, as necessary. A small amount (0.5–1 g) of Amberlite IR120 H resin, extensively prewashed with deionized water, was added to the solution and the mixture stirred for 1 min. When the pH reached 6.0–6.5, the resin beads were removed by filtration. The solution was adjusted to pH 8.5 with dilute sodium hydroxide and stirred on ice under reduced pressure overnight to remove any traces of organic solvent. The concentration of the stock solution was assayed by adding 10 μL of the *p*NPP solution to 1 mL of 100 mM Tris buffer (pH 10) followed by complete hydrolysis with alkaline phosphatase. The final concentration of liberated *p*-nitrophenol was found using a λ_{400} value of $18300\text{ M}^{-1}\text{ cm}^{-1}$.

Quantification of Inorganic Phosphate. A malachite green assay was used to determine the concentration of inorganic phosphate in the *p*NPP substrate, and the concentration of inorganic phosphate in inhibition studies. Briefly, 1.5 g of ammonium hexamolibdate was dissolved in 85 mL of deionized water. The volume was adjusted to 100 mL with 15 mL of concentrated (60.5%) perchloric acid yielding solution A. The use of perchloric acid was found to improve the sensitivity and rate of color development. Malachite green hydrochloride (0.2 g) was added to 50 mL of solution A while the mixture was being stirred. After 30 min, the dark orange solution was centrifuged to separate any undissolved particles yielding solution B. Solution A was used to adjust solution B to a final A_{450} of 15 (measured by assaying diluted aliquots and calculating back to the original concentration). In a separate 250 mL Erlenmeyer flask, 2.5 g of hydrolyzed PVA (Acros) was

stirred in 100 mL of deionized water while the mixture was being gently heated, avoiding boiling for several hours to yield clear colorless solution C [2.5% (w/v)]. Prior to use, 2 mL of solution C was added to 10 mL of adjusted solution B and the solution mixed to yield a dark brown working solution. In a 96-well plate, 280 μL of the working solution was mixed with 30 μL of diluted phosphate standards in the range of 0–200 μM . The color was fully developed in 3–5 min, and the absorbance measured at 625 nm was plotted versus inorganic phosphate concentration to obtain a calibration curve.

Determination of Inhibition Constants. The effect of buffers and other inhibitors on the activity of VHZ was tested with *p*NPP (sodium salt) in 50 mM sodium acetate buffer (pH 5.5), which showed no inhibitory effect, with inhibitor concentrations in the range of 25–200 mM. The data were fit to several inhibition models using a nonlinear least-squares fit (Origin 8.5.1) with the competitive model yielding the best results in all cases.

Steady-State Kinetic Analysis. All reactions were performed in noninhibitory buffers in the presence of 1 mM DTT and a constant ionic strength adjusted to 150 mM with NaCl at 25 $^{\circ}\text{C}$. The following buffers, which showed no inhibition against VHZ, were used: sodium acetate at pH 4.75–5.5, sodium succinate at pH 5.75–6.5, and 3,3-dimethylglutarate at pH 6.75–7.25. All buffers were at a concentration of 50 mM. At least eight substrate concentrations ranging from $0.5K_M$ to $4K_M$ were used for each enzyme to obtain Michaelis–Menten curves. Reaction progress was followed continuously by the change in absorbance at 400 nm at each pH using a VersaMax plate reader (Molecular Devices). Partial extinction coefficients obtained as described in the Supporting Information were used to convert the measured absorbance values into amounts of *p*-nitrophenol released. VHZ was susceptible to product inhibition, so linear initial velocities were used at each substrate concentration. Control reactions in the absence of enzyme verified that nonenzymatic hydrolysis could not be detected during the time spans used for enzyme kinetics. The initial rates were plotted versus substrate concentration and fit to the Michaelis–Menten equation using Origin version 8.5.1 to obtain kinetic parameters k_{cat} and K_M . The values of k_{cat} and k_{cat}/K_M were plotted versus pH and fit to the equations shown in the Supporting Information to obtain the $\text{p}K_a$ values of catalytically important ionizable residues, presented in the Table S1 of the Supporting Information.

Isotope Effect Measurements. Kinetic isotope effects (KIEs) on the VHZ-catalyzed reaction with *p*NPP were measured using the competitive method and thus are isotope effects on V/K . Figure 2 shows the positions at which KIEs were measured in the substrate and the designations used. Natural abundance *p*NPP was used for measurements of $^{15}(V/K)$. The ^{18}O KIEs $^{18}(V/K)_{\text{bridge}}$ and $^{18}(V/K)_{\text{nonbridge}}$ were measured by the remote label method, using the nitrogen atom in *p*-nitrophenol as a reporter of the isotopic fractionation in the labeled oxygen positions.¹³ The isotopic isomers used are shown in Figure 2, and their synthesis was as previously described.¹⁴ KIEs were measured at pH 5.5 using 100 mM acetate, 1 mM DTT, and 0.5 mM EDTA as a buffer. The reactions were conducted at 25 $^{\circ}\text{C}$ and 25 mM *p*NPP. All reactions for bridged, nonbridged, and natural abundance isotope effects were performed in triplicate, and the progress was monitored continuously by measuring the absorbance at 400 nm. Reactions were stopped at 40, 50, and 60% completion by acidification to pH 3.0 with HCl, which caused

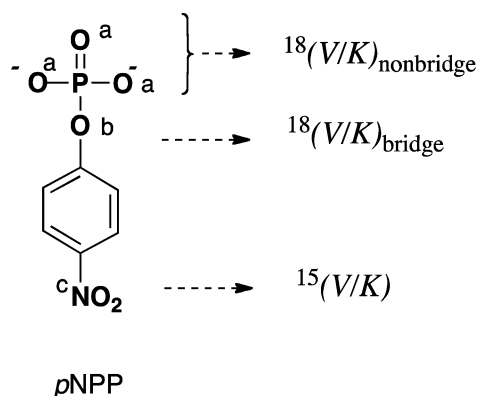


Figure 2. Positions of KIE measurement in the substrate *p*NPP. ^{18}O KIEs were measured at the nonbridging oxygen atoms of the phosphoryl group (a) and the bridging ester oxygen atom (b). The ^{15}N KIE was measured in the nitro group (c).

some precipitation of protein, which was separated by centrifugation. To remove the remaining enzyme, the reaction solution was centrifuged in a Millipore Amicon-Ultra 3 kDa protein concentrator. The resulting solution was extracted with three 50 mL portions of diethyl ether. Ether fractions were collected, dried with anhydrous magnesium sulfate, and filtered, and ether was removed by rotary evaporation. The unhydrolyzed *p*NPP remaining in the aqueous layer was hydrolyzed using alkaline phosphatase after the pH had been adjusted to 10 by addition of 1 M Tris to pH 11. After 8 h, the *p*NP product was extracted and collected as previously described. After sublimation, the *p*-nitrophenol samples were analyzed by isotope ratio mass spectrometry. The isotope effect was calculated from the nitrogen isotopic ratios in the *p*-nitrophenol product at partial reaction, in the residual substrate, and the starting material, as described in the Supporting Information. The $^{18}(\text{V}/\text{K})_{\text{nonbridge}}$ values were corrected for the dianionic fraction of *p*NPP at pH 5.5.

Detection of Phosphotransferase Activity in the Presence of Ethylene Glycol. The hydrolysis of *p*NPP by VHZ and VHZ/P68V was monitored using a JEOL 300 MHz NMR spectrometer at the 121.5 MHz ^{31}P resonance frequency. Reaction was started by addition of VHZ to a solution containing 20 mM *p*NPP in 50 mM sodium acetate (pH 5.5), 0.5 mM EDTA, 3 mM DTT, and 1 M ethylene glycol. The instrument was locked using D_2O in a coaxial tube. The instrument was set to collect 64 scans, with a relaxation delay of 4 s and a sweep width of 50 ppm.

The dependence of k_{cat} was measured as a function of ethylene glycol concentration for VHR, VHZ, VHZ/E134Q, VHZ/E134A, VHZ/D65A, VHZ/P68V, SsoPTP, and SsoPTP/V72P by monitoring the release of *p*-nitrophenol. Reactions were performed in 50 mM sodium acetate buffer (pH 5.5), and the concentration of ethylene glycol varied in the range of 0–3 M.

Pre-Steady-State Kinetics. Measurements of *p*NPP hydrolysis catalyzed by VHZ, VHR, and the VHZ/D65A mutant were performed at 25 °C using a stopped-flow spectrophotometer (KinTek). The release of *p*-nitrophenol was monitored by the increase in absorbance at 400 nm in 100 mM succinate buffer (pH 5.85), using an extinction coefficient corrected for this pH (see the Supporting Information). The enzyme concentration varied in the range of 20–65 μM . The *p*NPP concentration was 20 mM for VHZ/D65A and 50 mM

for VHR/WT and VHZ. Absorbance traces of at least five separate experiments at each substrate and enzyme concentration were averaged. The data were fit to the equation $[p\text{NPP}] = At + B(1 - e^{-kt})$. At saturating concentrations of substrate, $k = k_3 + k_5$. The linear steady-state phase $A = k_3k_5/(k_3 + k_5)$. The magnitude of the burst $B = \{E_0[k_3/(k_3 + k_5)]^2\}/(1 + K_M/S_0)^2$.

Computational Analysis of Binding of *p*NPP to VHZ.

The computational packages AutoDock^{15,16} and FlexX¹⁷ were used to model the docking of *p*NPP in the active site of VHZ. The 1.15 Å resolution crystal structure of the VHZ–metavanadate complex (PDB entry 4ERC) was used as the starting model. The VO_3 ligand at the active site was removed, and the following charges and protonation states were assigned to the residues: C95, –1; H94 and R101, +1; D65 and E134, neutral. The side chains of residues D65, F66, L97, and E134 were treated as flexible, and the rest of the protein was rigid. The *p*NPP ligand coordinates were extracted from the crystal structure of SsoPTP (PDB entry 2I6P), and the dianionic form of the phosphate ester was used for docking. Free rotation was allowed around the phosphate monoester bond, while the *p*-NPP ring was treated as planar and rigid. The Lamarckian genetic algorithm was selected for its reliability and ability to calculate “deeper minima”,¹⁸ and the search was conducted within a 15 Å grid region centered at the active site.

RESULTS

Buffer and Oxyanion Inhibition. The effects of buffers and oxyanions on the catalytic activity of VHZ are summarized in Table 1. No inhibitory effects were observed for acetate, succinate, 3,3-dimethylglutarate, or diglycine. VHZ is weakly

Table 1. Inhibition by Buffers and Oxyanions^a

compound	inhibition type	K_i (mM)
cyclohexylamine	competitive	140 ± 10
EDTA	competitive	22 ± 2
Inorganic Phosphate		
VHZ/WT	competitive	0.67 ± 0.05
VHZ/D65A	competitive	0.43 ± 0.12
VHZ/D65N	competitive	0.68 ± 0.11
Sso/WT	competitive	0.54 ± 0.42
VHR/WT	competitive	0.7 ± 0.3
YopH/WT	competitive	4.4 ± 0.2
PTP1B/WT	competitive	3.7 ± 0.1
Other Oxyanions		
sulfate	competitive	4.6 ± 0.3
arsenate	competitive	0.13 ± 0.04
vanadate	competitive	0.0027 ± 0.0003
Buffers		
Tris	competitive	88 ± 9
<i>N</i> -ethylmorpholine (NEM)	no	no
Bis-Tris	competitive	122 ± 12
triethanolamine	competitive	52 ± 5
HEPES	competitive	26 ± 3
glycylglycine	competitive	118 ± 12
sodium acetate	no	no
sodium succinate	no	no
3,3-demethylglutarate	no	no

^aExperiments were conducted at pH 5.5 in 100 mM sodium acetate buffer where the ionized form of tested buffering agents dominates in solution.

inhibited by triethanolamine hydrochloride and cyclohexylammonium hydrochloride, while *N*-ethylmorpholine (NEM) hydrochloride displayed no inhibitory effect. As expected, the sulfonate-containing buffer HEPES showed relatively strong inhibition. Cyclohexylammonium is a common counterion for the commercially available substrate *p*NPP, and although its effect was relatively weak, the sodium salt was used in all experiments.

Kinetic Isotope Effects. The KIEs in the positions shown in Figure 2 for the VHZ-catalyzed hydrolysis of *p*NPP are listed in Table 2, together with previously reported KIEs for PTP1B

Table 2. Kinetic Isotope Effects of Native VHZ, PTP1B, and VHR

PTP name	$^{15}(V/K)$	$^{18}(V/K)_{\text{bridge}}$	$^{18}(V/K)_{\text{nonbridge}}$
VHZ	1.0013 ± 0.0004	1.0164 ± 0.0017	0.9986 ± 0.0008
PTP1B ¹⁰	1.0001 ± 0.0002	1.0142 ± 0.0004	0.9981 ± 0.0015
VHR ¹⁹	0.9999 ± 0.0004	1.0118 ± 0.0020	1.0003 ± 0.0003

and VHR. The $^{18}(V/K)_{\text{nonbridge}}$ KIEs for VHZ are very similar to these precedents,^{10,19} suggesting that, like these related enzymes, the VHZ-catalyzed reaction proceeds via a loose transition state. The $^{18}(V/K)_{\text{bridge}}$ KIE is higher in VHZ, and a significant magnitude for the $^{15}(V/K)$ isotope effect contrasts with the absence of a measurable KIE in this position in the other two phosphatases. Both observations are consistent with incomplete neutralization of the leaving group by the general acid in the transition state.

Steady-State Kinetic Analysis. Table 3 shows kinetic parameters k_{cat} , K_M , and k_{cat}/K_M for VHZ, VHR, YopH, PTP1B,

Table 3. Kinetic Data for Native VHZ, YopH, VHR, PTP1B, and SsoPTP and Selected Mutants with *p*NPP at pH 5.5 (optimum) and 25 °C^a

	k_{cat} (s ⁻¹)	K_M (mM)	k_{cat}/K_M (mM ⁻¹ s ⁻¹)
Native PTPs			
VHZ	3.92 ± 0.03	8.31 ± 0.71	0.47
VHR	3.1 ± 0.1	1.96 ± 0.11	1.59
SsoPTP	3.15 ± 0.05	4.31 ± 0.19	0.73
YopH	720 ± 25	0.98 ± 0.11	735
PTP1B	51.7 ± 0.9	0.12 ± 0.01	430
IPD Loop Mutations			
SsoPTP/V72P	2.61 ± 0.1	4.62 ± 0.43	0.56
VHZ/D65A	0.84 ± 0.12	0.22 ± 0.01	4.19
VHZ/D65N	3.42 ± 0.12	8.73 ± 0.68	0.39
VHZ/D65N/E134Q	0.027 ± 0.002	27.77 ± 4.15	0.001
VHZ/P64A	0.07 ± 0.04	32.92 ± 2.98	0.002
VHZ/P69A	0.09 ± 0.05	31.00 ± 3.80	0.003
VHZ/P68V	3.34 ± 0.06	5.88 ± 0.27	0.57
Q-Loop			
VHZ/E134Q	0.42 ± 0.07	7.66 ± 0.25	0.07
VHZ/E134A	0.29 ± 0.02	10.15 ± 1.32	0.03
VHZ/Q138A	0.13 ± 0.01	13.1 ± 1.7	0.01

^aValues are the results of at least six independent experiments.

SsoPTP, and several VHZ mutants, measured at pH 5.5 and 23 °C. This corresponds to the pH optimum of many PTPs, including VHZ. The kinetic parameters for VHR, YopH, and PTP1B measured by a continuous assay at 400 nm are in good agreement with the literature values. We obtained a k_{cat} of 3.9

s⁻¹ and a K_M of 8.3 mM for *p*NPP hydrolysis by VHZ at the pH optimum of 5.5, compared with a previously reported k_{cat} of 0.009 s⁻¹ and a K_M of 1.5 mM.²⁰ The revised k_{cat} is comparable to those of native VHR and SsoPTP. The K_M is significantly higher than those values previously reported, resulting in a lower overall enzymatic efficiency (k_{cat}/K_M).

pH Dependence for the Hydrolysis of *p*NPP by VHZ.

The pH–rate profiles for native VHZ and mutants D65A and E134Q are shown in Figure 3. The pK_a values of ionizable residues were determined by nonlinear least-squares fitting of experimental data to the appropriate equations (see the Supporting Information), for k_{cat} and k_{cat}/K_M , and are listed in Table S1 of the Supporting Information. The second ionization constant for *p*NPP was set to the literature value of 4.96.¹² The pK_a values obtained are in good agreement with those previously obtained for other PTPs, and the bell-shaped profiles are typical of the PTP family. The acid limb is ascribed to the deprotonated C95 nucleophile, which has an unusually low pK_a because of the stabilizing influences of the neighboring H94 in VHZ. The basic limb is ascribed to general acid catalysis in the first step, consistent with the PTP mechanism (Scheme 1).

The IPD loop in VHZ bears the putative D65 general acid. This loop and the position of the acid correspond to the conserved WPD loop in classical PTPs (Figure 4). D65 was proposed to be the general acid catalyst by structural analogy, and on the basis of the observation of lost hydrolysis of *p*NPP by the D65A mutant.^{21,22} In our hands, the D65A mutation resulted in a 5-fold decrease in k_{cat} and a 40-fold decrease in K_M . The pH–rate profile remains bell-shaped (Figure 3). In contrast, the analogous mutation of the general acid in other PTPs to alanine or to asparagine results in a 100–1000-fold decrease in k_{cat} , and the loss of the basic limb in the kinetic pH–rate profile, indicating loss of general acid catalysis.^{23,24} In contrast, the kinetic constants for the D65N mutant are similar to those of native VHZ (Table 3).

The active site of VHZ possesses another acid (E134 from the Q-loop) in position to potentially protonate the leaving group (Figure 4). The E134Q and E134A mutations both decreased k_{cat} by approximately 1 order of magnitude (Table 3) with no significant effect on K_M . The pH–rate profile of the E134Q mutant remained bell-shaped. Only the simultaneous removal of both general acids (D65N/E134Q) led to a significant decrease in k_{cat} and the loss of the basic limb of the pH–rate profile (Figure 3). The double mutant precipitated below pH 5.25, precluding measurement of kinetic data below this pH.

Pre-Steady-State Kinetics. Many PTPs, including YopH, PTP1, and VHR, exhibit burst kinetics, indicating that the second step is rate-limiting.^{3,25} When native VHR was rapidly mixed with *p*NPP, a pre-steady-state burst of *p*-nitrophenol release was observed (Figure 5).

The values of k_3 and k_5 obtained for VHR are close to those previously reported.²⁵ Under the same conditions, native VHZ and its E134Q mutant revealed no pre-steady-state burst. In contrast, the VHZ/D65A mutant displayed a pre-steady-state burst that was stoichiometric with the amount of enzyme. Values of k_3 , k_5 , and K_5 (the true substrate binding constant) were calculated for native VHR and VHZ/D65A and are listed in Table 4. Although the decrease in the ratio (k_5/k_3) in VHZ/D65A decreases K_M (see the Supporting Information), it does not fully explain the magnitude of the reduction, indicating that K_5 is decreased, as well. Despite the absence of a burst, the

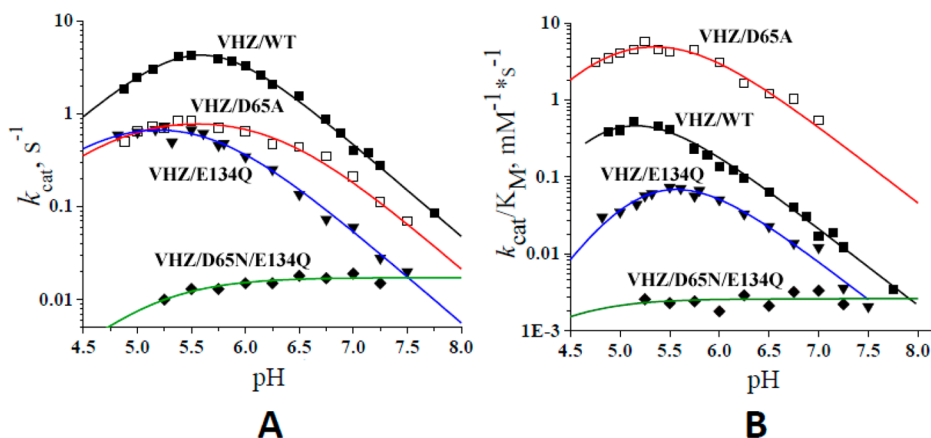


Figure 3. pH–rate profiles. (A) k_{cat} values for native VHZ (black) and its D65A (red), E134Q (blue), and D65N/E134Q (green) mutants. (B) k_{cat}/K_M values for native VHZ and its D65A, E134Q, and D65N/E134Q mutants. The D65A mutant is more efficient than native VHZ because of the simultaneous reduction of k_{cat} and K_M . Both D65A and E134Q mutants retain the basic limb diagnostic of general acid catalysis. The basic limb completely disappears in the VHZ/D65N/E134Q double mutant.

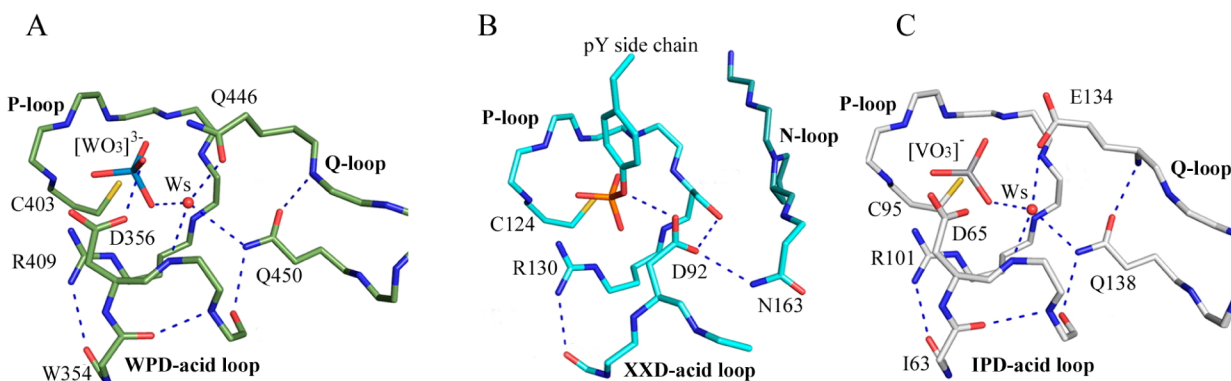


Figure 4. Structural comparison of the active sites of (A) the YopH PTP, (B) the VHR DSP, and (C) VHZ PTP. The structural arrangement of the VHR active site differs from that of YopH and VHZ in the replacement of the highly conserved Q-loop with the N-loop, and a different position of the general acid.

value of K_S for native VHZ can be calculated if we assume that the primary role of D65 is orienting the nucleophilic water in the second step. This assumption is supported by the negligible effect on k_{cat} of the D65N substitution. By setting k_3 for native VHZ equal to that of D65A, we calculated the other elementary rate constants for the reaction of the native enzyme as shown in Table 4. The VHZ/D65A substitution decreases the magnitude of K_S 14-fold. Because substitution of D65 with A (but not N) increases the enzyme substrate affinity, we conclude the existence of an unfavorable steric, rather than electrostatic, interaction between D65 and the aromatic ring of the substrate. The K_i for inorganic phosphate is lower than the K_S for *p*NPP in both native VHZ and VHZ/D65A. However, whereas the K_S for *p*NPP is decreased 14-fold by the removal of the D65 side chain (Table 4), the K_i for inorganic phosphate is decreased only ~ 1.5 -fold (Table 1).

Reaction in the Presence of Ethylene Glycol. The dependence of k_{cat} on ethylene glycol concentration was measured for native VHZ and several mutants. It should be noted (discussed in the Supporting Information) that the slope of such a plot where $k_{cat} = k_5 + k_7[\text{ROH}]$ yields the second-order rate constant for ethylene glycol phosphorylation [k_7 (Scheme 2)] only when $k_3 \gg k_5$. In the more general case, when no distinct rate-limiting step exists and no pre-steady-state burst is present, the expression $k_{cat} = (k_3k_5)/(k_5 + k_3) +$

$((k_3k_7)/(k_5 + k_3)) \times [\text{ROH}]$ holds and interpretation of the calculated slope is more complex. However, the nucleophilic selectivity $S = \text{slope}/\text{intercept} = [(k_3k_7)/(k_5 + k_3)]/[(k_3k_5)/(k_5 + k_3)] = k_7/k_5$ (Table 5, column 3) is independent of k_3 and reflects the relative preference for alcoholysis over hydrolysis.

The E134Q mutation results in no significant change in phosphotransferase ability. The E134A mutation increases the alcoholysis to hydrolysis ratio, indicating that E134 participates in the second step of the reaction, like Q446 in YopH. Although Q-loop residues in PTPs are generally thought to control access to the phosphoenzyme intermediate, the D65A mutation on the IPD loop has a more pronounced effect than the E134A mutation. Because the closely related SsoPTP lacks phosphotransferase activity, we compared the effects of mutations on the IPD loops in VHZ and SsoPTP. The SsoPTP contains only two proline residues on its IPD loop, P68 and P73, corresponding to P64 and P69, respectively, in VHZ. These residues are highly conserved in classical PTPs (see the sequence alignment in Figure 8), and mutations result in similar, adverse catalytic effects in VHZ (Table 3). VHZ possesses another proline, P68, which is occupied by V72 in SsoPTP. The VHZ/P68V mutation abolished phosphotransferase activity (Figure 6). This effect was further supported by ^{31}P NMR spectroscopy shown in Figure 7. The orthogonal

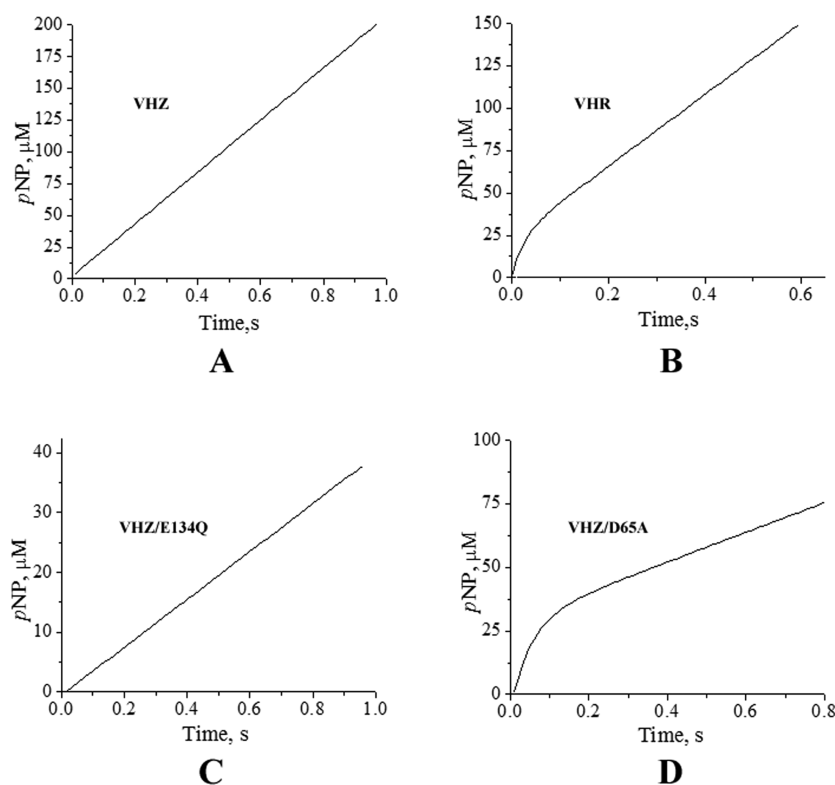


Figure 5. Pre-steady-state kinetics of (A) 48 μM native VHZ with 50 mM $p\text{NPP}$, (B) 26 μM native VHR with 50 mM $p\text{NPP}$, (C) 58 μM VHZ/E134Q with 50 mM $p\text{NPP}$, and (D) 28 μM VHZ/D65A with 10 mM $p\text{NPP}$. All experiments were performed at 25 $^{\circ}\text{C}$; 2000 data points were collected after a 1 ms mixing delay and used in the fit. Data points were omitted from the figure for the sake of clarity.

Table 4. Elementary Rate Constants for $p\text{NPP}$ Hydrolysis and Substrate Dissociation Constants for Native VHR, VHZ/D65A, and Native VHZ^a

	k_3 (s^{-1})	k_5 (s^{-1})	K_S (mM)
VHZ/D65A	17.44 ± 0.13	1.71 ± 0.37	2.5
VHR	48.30 ± 0.34	9.70 ± 0.21	11.8
VHZ/WT	17.44 ± 0.13	5.19	35

^aThe values of k_3 , k_5 , and K_S were obtained from burst kinetics as described in the Supporting Information. The kinetic constants for native VHZ were calculated on the basis of the assumption that k_3 is not affected by the VHZ/D65A substitution, as described in the text. Under such circumstances, the system consisting of the two equations $k_{\text{cat}} = (k_3 k_5) / (k_3 + k_5)$ and $K_M = K_S [k_5 / (k_3 + k_5)]$ can be solved to obtain values of k_5 and K_S .

SsoPTP/V72P mutation conferred phosphotransferase ability comparable to that of native VHZ.

DISCUSSION

Although VHZ is related to classical PTPs and utilizes the same mechanism,⁸ it differs in several important ways from most PTP family members.

VHZ Is Inhibited by Commonly Used Buffers and by Inorganic Phosphate More Strongly Than Typical PTPs.

Previous kinetic investigations of VHZ utilized single-time point assays after 20 or 30 min and buffers containing Tris^{20,22} or Bis-Tris, which are weak competitive inhibitors (Table 1). Although the inhibition constants are in the high millimolar range, buffers are typically used at such concentrations. While buffers containing the sulfonate functional group, such as HEPES, are recognized as inhibitors of PTPs and have been

Table 5. Second-Order Rate Constants for Alcoholysis and Hydrolysis of $p\text{NPP}$ by Several Members of the PTP Family^a

name	k_t ($\text{M}^{-1} \text{s}^{-1}$)	$k_{\text{cat}}' = k_{\text{cat}} / 55.5$ ($\text{M}^{-1} \text{s}^{-1}$)	$S = k_t / k_{\text{cat}}'$
Ltp1/WT ⁷	5.5	0.026	211.5
YopH/WT ⁶	0.0	11.3	0.0
SsoPTP/WT	0.0	0.07	0.0
VHR/WT ⁶	0.48	0.07	6.85
VHZ/WT	1.3	0.09	14.4
VHZ/E134Q	0.06	0.005	12.1
VHZ/E134A	0.13	0.0036	36.1
YopH/Q446A ⁶	21.6	1.11	19.4
VHZ/D65A	1.55	0.015	103.3
VHZ/P68V	0.0	0.060	0.0
SsoPTP/V72P	0.49	0.041	11.95

^aThe k_{cat} values obtained in the absence of alcohol (intercept with the Y axis) were divided by the molarity of water (55.5 M) to yield the second-order hydrolysis rate constant k_{cat}' . Nucleophilic specificity is defined by the relative preference for alcoholysis over hydrolysis. k_t corresponds to k_7 only when $k_5 \gg k_3$; otherwise, $k_t = (k_3 k_7) / (k_5 + k_3)$ (see the Supporting Information for a more detailed description). The values of k_t depend on the rate-limiting step and on the overall activity and should not be used to judge the preference for alcoholysis.

observed in some PTP crystal structures, the inhibition of VHZ by buffers such as Tris and triethanolamine was unexpected. This behavior may result from the combined effect of several anionic residues near the VHZ active site (D65, E44, E134, and E137), but the molecular origin of buffer inhibition was not tested. The inhibition constant for inorganic phosphate is lower than in classical PTPs and is significantly lower than the K_S for $p\text{NPP}$ (Table 4). Probable structural origins for this difference

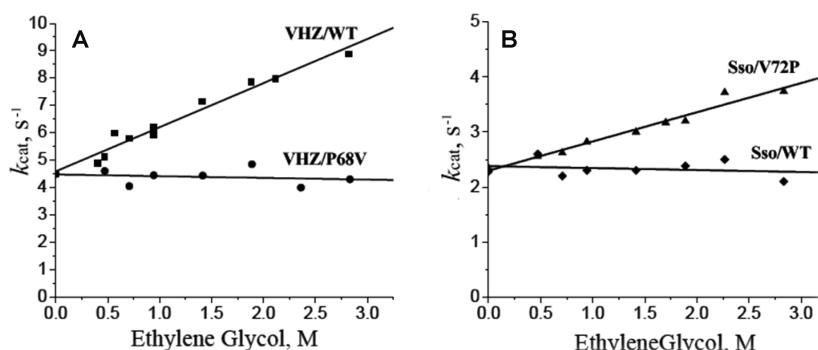


Figure 6. Dependence of *p*NPP turnover on ethylene glycol concentration for (A) VHZ/WT and the VHZ/P68V mutant and (B) SsoPTP/WT and the SsoPTP/V72P mutant. The k_{cat} for *p*NPP release was plotted vs ethylene glycol concentration. All experiments were performed at 25 °C.

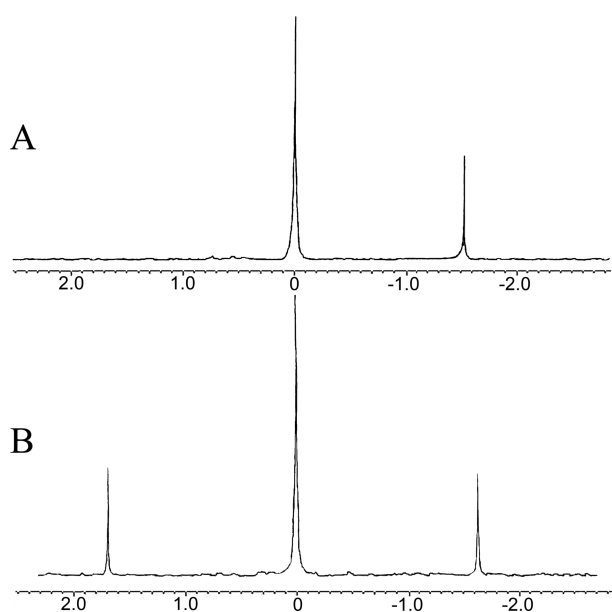


Figure 7. Reaction of *p*NPP catalyzed by VHZ/P68V and VHZ monitored by ^{31}P NMR spectroscopy. Panel A shows the reaction of the VHZ/P68V mutant after 30 min in the presence of 1 M ethylene glycol. Panel B shows the reaction catalyzed by VHZ after 30 min. All reactions were performed at pH 5.5 in 100 mM sodium acetate buffer in the presence of 20 mM *p*NPP. The chemical shift of *p*NPP was -1.6 ppm; that of inorganic phosphate was set to 0 ppm, and the shift of phosphorylated ethylene glycol is 1.7 ppm.

are discussed below. The net effect of these properties led to a significant underestimation of VHZ activity in previous reports.

In addition to avoiding inhibitory buffers, we validated a method for the continuous collection of rate data using the substrate *p*NPP monitoring reaction progress at 400 nm using extinction coefficients measured under the experimental conditions (see the Supporting Information). Continuous monitoring of the reaction showed that VHZ becomes inhibited by the product after several minutes. Finally, commercial *p*NPP, which often contains small but experimentally significant amounts of inorganic phosphate, was used in previous studies. We developed a purification strategy to minimize contamination by inorganic phosphate, which also offers a simple means of converting the dicyclohexylammonium salt to the more soluble disodium salt.

Using noninhibitory buffers, a continuous assay, and phosphate free substrate, VHZ proved to be significantly more active than previously reported ($k_{\text{cat}} = 3.9 \text{ s}^{-1}$ vs a

previous published value of 0.009 s^{-1}). We also developed a process for the expression and purification of the native enzyme with no tags. Although previous reports used tagged versions of VHZ, the difference in activity is too significant to be explained by the absence of tags. Furthermore, discontinuous assays of tagless VHZ using the previously reported methods yielded results similar to those of previous reports.^{20,22}

The Leaving Group Is Not Fully Neutralized in the First Step of the VHZ Reaction. The KIEs for the hydrolysis of *p*NPP have been reported for a number of PTPs, including YopH,²⁶ PTP1B,²⁷ VHR,¹⁹ and the LMW PTP Stp1.²⁸ Because these are measured by the competitive method, the KIEs reflect the portion of the kinetic mechanism up to the first irreversible step, cleavage of *p*NPP. The mechanistic origins of the KIEs for *p*NPP hydrolysis have been described elsewhere.¹³ In brief, a normal $^{15}\text{V}/\text{K}$ up to a maximum of 1.003 arises from negative charge development on the leaving group. Efficient general acid catalysis by PTPs abolishes this effect, resulting in a $^{15}\text{V}/\text{K}$ of unity. Fission of the P–O bond produces a normal $^{18}\text{V}/\text{K}_{\text{bridge}}$ effect. Simultaneous leaving group protonation produces an inverse effect that partially decreases the normal effect from P–O cleavage. Thus, in general acid mutants, $^{18}\text{V}/\text{K}_{\text{bridge}}$ is typically ~ 1.03 , compared to ~ 1.015 in native PTPs. The $^{18}\text{V}/\text{K}_{\text{nonbridge}}$ KIE responds to the change in the hybridization state of the phosphoryl group. This KIE is slightly inverse to near unity in PTPs, reflecting the loose metaphosphate-like transition state; associative transition states result in normal values.

Both of the oxygen isotope effects for the VHZ reaction are within experimental error of previous data with PTP1B and VHR (Table 4). In contrast, the $^{15}\text{V}/\text{K}$ differs from those of the other PTPs and is slightly normal, indicating that the leaving group is not completely neutralized in the transition state. The magnitude suggests approximately one-third of a negative charge, from protonation that is not fully synchronous with P–O bond fission. This has been observed in one previous PTP family member, the LMW PTP Stp1.²⁸ Incomplete protonation of the leaving group in the first step may contribute to a decrease in k_3 and explain the absence of a burst in the VHZ-catalyzed reaction of *p*NPP.

Two Potential and Functional General Acids in the Active Site of VHZ. The D65 residue resides on the IPD loop, a structure analogous to the WPD loop in classical PTPs that bears the conserved general acid (Figure 8). The E134 residue in VHZ can be superimposed with a conserved Q residue located on the Q-loop in classical PTPs that orients the nucleophilic water in the second step.²⁹ The pH–rate profiles

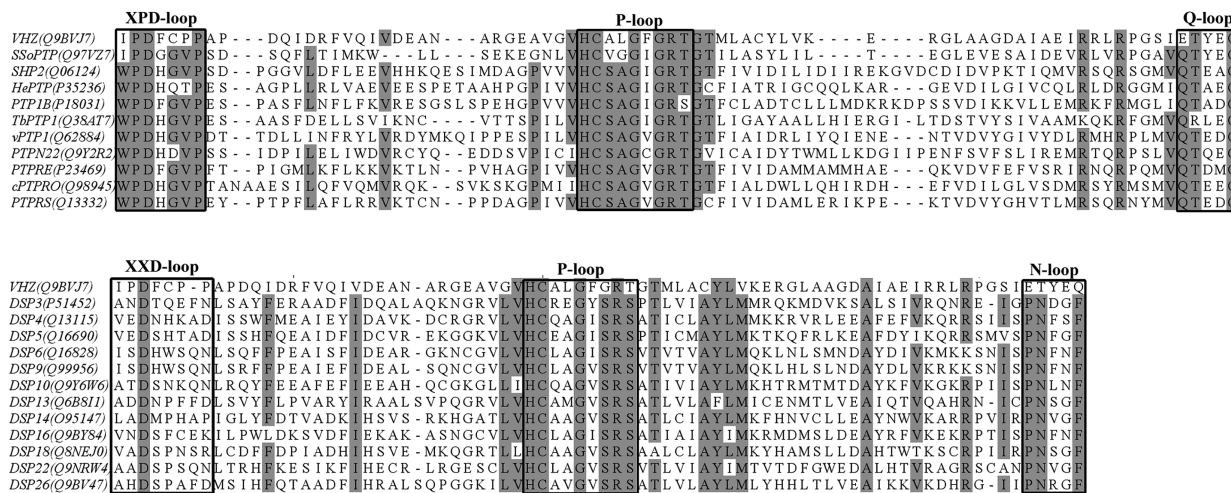


Figure 8. Sequence alignment of residues 65–138 of VHZ with several classical PTPs (top) and atypical DSPs (bottom). The alignment is confined to the three catalytically important PTP regions, as they are most similar in sequence in the PTP family. VHZ is more similar to classical PTPs than to the DSP family, with two important distinctions in the aligned regions: substitution of highly conserved W by I in the WPD loop region and substitution of Q by E in the Q-loop region.

of the D65 and E134 mutants both retain their basic limbs. The D65N mutation has no significant effect on catalysis, and the D65A and E134Q mutations have k_{cat} values that are decreased by only 1 order of magnitude. Only in the double mutant is the level of catalysis decreased to the extent seen in general acid mutants of other PTPs, consistent with complete elimination of general acid catalysis. We conclude the D65 and E134 single mutants both retain general acid function. We conclude that native VHZ utilizes E134 as the primary general acid, with a minor contribution from D65, which becomes the major general acid when E134 is mutated. The data suggest that, unlike any other known PTP or DSP, VHZ contains two acidic residues in the active site, either of which can protonate the leaving group in the absence of the other.

One might consider whether these results arise from the good leaving group in *p*NPP that may not need an enzymatic general acid to protonate it at the acidic pH optimum. However, several lines of evidence show that general acid catalysis is part of the mechanism of *p*NPP hydrolysis by PTPs, as with other substrates. KIE results at the acidic pH optima across the PTP family show that the leaving group leaves as the neutral phenol in native enzymes but is charged when the enzymatic general acid is mutated. In such mutants, the rates of *p*NPP hydrolysis are significantly decreased, and pH–rate profiles lose their basic limbs.¹³

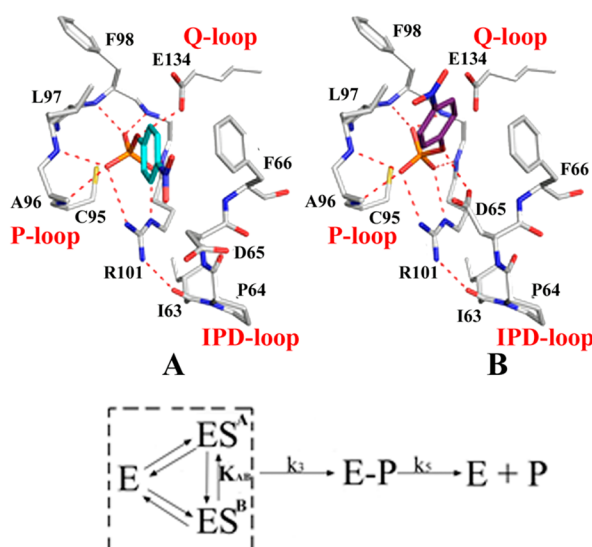
D65 Has a Role Primarily in the Second Step and Affects Substrate Binding. The fact that the D65N mutation does not significantly affect activity, while the D65A mutation does, suggests that the reduced level of catalysis in the D65A mutant arises because of the inability of the alanine side chain to participate in phosphoenzyme hydrolysis by orientation of the nucleophilic water. In this sense, the roles of D65 and E134 are reversed from those of classical PTPs, in which the conserved glutamine corresponding to E134 positions the nucleophilic water and the acid corresponding to D65 is the general acid in the first step and the general base in the second step.

The D65A mutation significantly decreases K_M and K_S . This effect is less pronounced for mutations of the corresponding residue in other PTPs. This may be explained by fact that in classical PTPs this residue resides on the mobile WPD loop,

which is primarily in an open conformation in the free enzyme. Because the IPD loop in VHZ is permanently closed,⁸ the D65 side chain is fixed in a position that restricts access to the deep and narrow VHZ active site. DSPs, such as VHR, also have a nonmovable general acid loop; however, in these enzymes, the general acid is positioned on another side of the active site (Figure 4) and presents less steric hindrance to incoming ligands. This explains the higher K_M for *p*NPP in VHZ compared to other PTPs. The structurally analogous SsoPTP, which also contains a rigid IPD loop, has a K_M value approximately 2-fold lower than that of VHZ and comparable to that of VHR. However, unlike the active site of VHZ, which has a narrow and deep pocket,⁸ the active site of SsoPTP is broad and shallow because of the presence of multiple surrounding glycine residues in the P-loop and IPD loop (Figure 8).

Neither the D65A nor the D65N substitution significantly affects the K_i for inorganic phosphate (Table 1). It also confirms that the mutation of the D65 side chain does not disrupt the P-loop, which serves as the dominant binding element to the anionic phosphoryl group. In contrast, the D65A mutation decreases the K_S for *p*NPP 14-fold. This suggests the effect of D65 substitutions on binding is primarily steric rather than electrostatic, involving the ester group of the substrate more than the phosphoryl group. This would permit the biological activity of VHZ to be more regulated by levels of intracellular phosphate than the activity of most classical PTPs. The intracellular regulation of phosphatases by phosphate has been recently discussed.³⁰ Unlike classical PTPs with much higher K_i values, VHZ, SsoPTP, and VHR have inhibition constants similar to the average physiological concentration of inorganic phosphate (1–1.3 mM).³¹

VHZ Has a Low Catalytic Efficiency and Different Rate-Limiting Step Compared to Those of Most PTPs. Despite the fact that VHZ is more active than previously thought, it remains one of the least active PTPs. A significant part of its decreased catalytic efficiency arises from its high K_S . Indeed, for the PTP-catalyzed reaction (Scheme 1), $k_{cat}/K_M = k_3/K_S$ (see the Supporting Information for derivation), which means that VHZ requires a 5–8-fold higher substrate concentration to achieve its limiting velocity. In addition to



$$V_{\max}^A + V_{\max}^B = V_{\max}^{\text{WT}} \times \alpha_A + V_{\max}^{\text{WT}} \times \alpha_B = V_{\max}^{\text{WT}} \times (\alpha_A + \alpha_B) = V_{\max}^{\text{WT}} \times 1 = V_{\max}^{\text{WT}}$$

Figure 9. Two *p*NPP docking modes in the active site of VHZ predicted by docking studies. In mode A, the scissile ester oxygen of the *p*NPP substrate is oriented toward the E134 side chain. Acid catalysis by D65 is not possible, as its side chain is displaced to relieve a steric clash with the substrate. The D65A mutation removes this clash, explaining its lower K_M . When E134 is mutated, general acid catalysis by D65 can occur from the binding mode shown in mode B. Conformation B is analogous to that observed in the crystal structure of the substrate bound to an inactive mutant of SsoPTP and is consistent with the pH–rate profile of E134Q.

high K_S values, the k_{cat} for VHZ is lower than those of classical PTPs. Our data suggest that both steps of the VHZ-catalyzed reaction are slower than in classical PTPs, and both contribute to the overall rate [$k_{\text{cat}} = (k_3 k_5) / (k_3 + k_5)$] under steady-state conditions. According to the KIE results, the neutralization of the leaving group in the first step is incomplete, which decreases k_3 but cannot explain the decrease in k_5 . It was previously shown that mutations of Q-loop residues in classical PTPs decrease k_5 by 2 orders of magnitude, an effect that was used to trap the phosphoenzyme intermediate of PTP1B.^{24,29} The E134Q mutation makes VHZ structurally more similar to classical PTPs and affects only the first step, resulting in the 8-fold decrease in activity. The k_{cat} value of the E134A mutant is 70% of that of the E134Q mutant. Such an insignificant decrease from complete removal of the functional group indicates that the residue does not function in the second step like the Q in this position in classical PTPs, explaining the lower k_5 in VHZ compared to those of other PTPs. The k_5 value of native VHZ is more similar to that of VHR (Table 4), which in place of the Q-loop (Figure 4) has an N-loop region (Figure 8) that is highly conserved among atypical DSPs.

VHZ Has Two Substrate Binding Modes for *p*NPP. The expressions for k_{cat} and K_M for the PTP-catalyzed reaction (Scheme 1) [$k_{\text{cat}} = (k_3 k_5) / (k_3 + k_5)$, and $K_M = K_S [k_5 / (k_3 + k_5)]$] contain the same elementary constants, and thus, any change in k_{cat} is reflected in K_M and vice versa. A decrease in k_3 results in an increased K_M as is seen in the VHZ/E134Q/D65N double mutant, in which both general acids important in k_3 are mutated but k_5 remains unaffected. As k_3 becomes smaller than k_5 , K_M approaches K_S . Because of this, the K_M for the VHZ/D65N/E134Q double mutant (Table 3) is close to the K_S for native VHZ determined from pre-steady-state kinetics (Table 4). The same effect has been previously observed in the general acid D92N mutant of VHR.²³ In contrast, mutations of Q-loop

residues that do not affect k_3 but decrease k_5 have the opposite effect on K_M . The same trend was previously observed in the Q556M and Q446A mutants of YopH.⁶ The decrease in k_5 reduces the rate of formation of the free enzyme form E, which lowers the K_M parameter in the steady-state experiment. This mutual dependence of k_{cat} and K_M becomes less obvious when $k_3 \gg k_5$, but because in native VHZ the two constants are relatively similar (consistent with the absence of a burst), even small changes should be easily detected. The E134Q mutation in VHZ eliminates the major general acid but results in an only 10-fold decrease in k_{cat} and has no effect on K_M . The D65N substitution results in a modest rate reduction, consistent with its role as the minor general acid, but also has no significant effect on K_M . The pH–rate profiles of both mutants remain bell-shaped, indicating that when one general acid is eliminated, the other one remains, maintaining general acid catalysis. The kinetic behavior of the mutants suggests the presence of two catalytically equivalent, but differently populated, forms of the Michaelis complex. Similar to the mode of action of a noncompetitive inhibitor on the native enzyme, the E134Q or D65N mutation renders one of the two conformations catalytically unproductive, which decreases the rate but has no effect on K_M .

To gain insights into substrate binding modes in VHZ that might explain how either D65 or E134 can act as a general acid, AutoDock^{15,16,32,33} and FlexX¹⁷ were used to predict the orientation of *p*NPP in the active site. Both programs predicted two possible conformations, presented in Figure 9. In each, the phosphate moiety of the substrate is coordinated by the P-loop and the side chain of R101 and is properly positioned for nucleophilic attack by the negatively charged cysteine at the bottom of the active site. In conformation A, the scissile oxygen is oriented toward E134, consistent with its assignment as the primary general acid. The D65 side chain turns away to prevent

a steric clash with the *p*-nitrophenyl ring. We conclude that this substrate conformation is the predominant one, consistent with the kinetic effects of the E134Q mutation and steric relief observed in the D65A mutant. The substrate conformation in Figure 9B is the one commonly observed in classical PTPs, except for the position of the glutamine residue analogous to E134, which occupies a different conformation to prevent a steric clash with the substrate phenyl ring.²⁹ However, it resembles the position of the corresponding Q135 residue in several structures of SsoPTP in complex with peptide substrates.⁹ In this conformation, the phenolate ring is close to the L97 side chain and D65 is oriented in a position to donate its proton to the scissile oxygen of the leaving group. This substrate orientation is consistent with the kinetic behavior of the E134Q mutant, which utilizes D65 as its general acid.

The presence of two binding conformations explains why the E134Q and D65N mutants have different effects on k_{cat} with no significant effect on K_{M} . If conformation B, in which the E134Q mutant can utilize the D65 general acid, presents a minor fraction of the overall enzyme–substrate complex, then it would kinetically appear as a decrease in k_{cat} because the predominant conformation A would be catalytically unproductive in this mutant. The different effects of the D65N and E134Q mutations on k_{cat} with no significant effect on K_{M} suggest that while both conformations A and B coexist, conformation A dominates. The E134Q or D65N substitution, which results in conformation A or B becoming nonproductive, respectively, is similar to the effect from noncompetitive inhibition. Noncompetitive inhibition results from the formation of a nonproductive enzyme–substrate–inhibitor complex that decreases V_{max} but has no effect on K_{M} . The reaction is catalyzed by the E134Q mutant in which conformation A is unproductive and conformation B leads to product formation according to the equation $V_{\text{max}}^{\text{A}} = V_{\text{max}}^{\text{WT}} / (1 + 1/K_{\text{AB}})$, where $V_{\text{max}}^{\text{WT}}$ is the maximal rate of the reaction with native VHZ and $V_{\text{max}}^{\text{A}}$ is the maximal velocity with the E134Q mutant. The calculated value of $K_{\text{AB}} = [\text{B}]/[\text{A}] = 0.12$ indicates that ~89% of the VHZ [ES] complex exists in conformation A and 11% in form B. This ratio is consistent with the modest decrease in k_{cat} in the D65N mutant. The equilibrium constant of 0.12 implies a modest energetic difference of slightly more than 1 kcal/mol, consistent with the nearly equal scoring function obtained from the docking programs for the two conformations.

The predominance of conformation A in which the phenolate ring interacts with the D65 side chain explains the steric relief produced by the D65A mutation. The presence of the E134 general acid and its use in conformation A may be a reasonable evolutionary solution to permit a bulky substrate to enter the narrow and sterically demanding active site pocket. Conformation B is the one the most commonly observed in the classical PTPs, which possess a movable WPD loop. This conformation allows VHZ to utilize its D65 general acid. However, under the condition of a nonmovable general acid-bearing loop, conformation B is sterically disfavored, making it less populated than conformation A. The presence of the two coexisting but unequally populated conformations explains why both the E134Q and D65N mutants retain their basic limbs in the pH–rate profile but produce a proportionally different effect on k_{cat} without affecting K_{M} .

A similar phenomenon may explain anomalous behavior reported in the Tk-PTP, a protein tyrosine phosphatase isolated

from *Thermococcus kodakaraensis* KOD1. On the basis of structural comparisons with known PTPs, D63 was assigned as the putative general acid. Unexpectedly, the D63A mutant was found to be more active, not less, than the native enzyme.³⁴ No structure of Tk-PTP has been published; however, the protein sequence (Figure S2 of the Supporting Information) suggests the presence of a glutamic acid residue in a position corresponding to that of E134 in VHZ. Like VHZ, Tk-PTP may utilize a general acid different from the one implicated by structural comparisons with the PTP family.

The finding of two alternate binding modes and two general acids may be physiologically relevant, but the results presented here do not address whether the same flexibility pertains to peptide substrates. Physiological substrates for VHZ have not been confirmed. Recently, the existence of two alternate peptide substrate binding modes, depending on sequence, has been reported for the related enzyme, VHR.³⁵ In that case, only a single general acid is in the active site and is used in both conformations.

VHZ Exhibits Phosphotransferase Activity Controlled by a Single Residue on the IPD-Loop. In classical PTPs, Q-loop residues such as Q446 and Q450 in YopH (Figure 4), in locations analogous to E134 and Q138 in VHZ, position the nucleophilic water for the second step and shield the phosphoenzyme from larger nucleophiles.⁶ In classical PTPs, catalysis is unaffected by added ethylene glycol. In contrast, YopH mutants in which these glutamines are mutated show significant phosphoryl transfer to ethylene glycol.⁶ This has provided a rationalization for why native VHR and LMW Ltp1, which lack an analogous Q-loop, display phosphotransferase activity.⁷ Thus, the observation of phosphotransferase activity by VHZ was unexpected, because its E134 and Q138 residues can be superimposed with Q446 and Q450 in YopH. The ratio S of the second-order rate constant for alcoholysis by ethylene glycol (k_t) to the hydrolysis of the phosphoenzyme intermediate (k_{cat}') is 14.4 (Table 5). This ratio was not significantly affected by the E134Q mutation, indicating that the E and Q residues, as was previously shown with YopH, are interchangeable.⁶ The higher level of transphosphorylation by the E134A mutant indicates that E134 provides some shielding of the phosphoenzyme. However, the analogous Q446A mutation in YopH results in a greater increase, from which we conclude that E134 in VHZ does not function as effectively in the second step as Q446 in YopH. The D65A substitution in VHZ results in the most pronounced increase in the S ratio, which, together with the decreased k_{cat} and presence of a pre-steady state burst, indicates that D65 is important in the second step.

Interestingly, unlike VHZ, there is no effect of ethylene glycol concentration on catalysis by SsoPTP. A sequence alignment of the IPD loops of VHZ and SsoPTP revealed that while SsoPTP contains two proline residues in this region, a pattern that is highly conserved in the PTP family, VHZ has a third proline, P68. In SsoPTP, V72 is found in the corresponding position. The P68V mutation in VHZ results in no significant change in k_{cat} ; however, phosphotransferase activity is lost, and there is no dependence of the rate on ethylene glycol concentration. The orthogonal V72P mutation in SsoPTP confers phosphotransferase ability similar to that of native VHZ. We thus conclude that the single-point mutation of proline at the P68 position in VHZ, and the analogous V72 position in SsoPTP, controls the ability of these enzymes to phosphorylate alcohols. Because the IPD loops in VHZ and

SsoPTP are not mobile, this mutation has no effect on k_{cat} . Further studies, including structural comparisons, are underway to seek an explanation of how this residue controls phosphotransferase activity.

CONCLUSIONS

Although VHZ is more closely related to classical PTPs than to DSPs, it is unique and has a number of unusual properties. VHZ has two functional general acids and, for the small molecule substrate *p*NPP, two substrate binding modes. Both binding modes are catalytically equivalent but unequally populated. Each binding mode utilizes a different general acid.

Despite the fact that VHZ shares many active site characteristics of classical PTPs, it is a significantly less efficient catalyst. Both catalytic steps k_3 and k_5 are slower. The decreased k_3 is consistent with incomplete neutralization of the leaving group revealed by KIEs. The decrease in k_5 is due to the less efficient involvement of the E134 residue in the second step, as revealed by the E134Q and E134A mutations.

The results also provide a rationale for the advantage of mobility of the general acid-bearing WPD loop in classical PTPs. The availability of an uncatalytic, open conformation allows the general acid to avoid sterically unfavorable interactions with substrate binding and to alleviate product release and decrease the level of product inhibition.

The discovery of phosphotransferase activity of VHZ also leads to several conclusions.

(1) The fact that the reaction rate increases linearly with ethylene glycol concentration indicates the second step is at least partially rate-limiting. Together with the absence of a burst in the presteady state, we conclude that both steps contribute to the overall rate.

(2) The Q-loop does not fully participate in protecting the active site from incoming alcohol nucleophiles. Mutations in the IPD loop of VHZ have a stronger effect on phosphotransferase ability. It is logical to conclude that the phosphotransferase activity observed in VH1-related DSPs and low-molecular weight PTPs can no longer be explained solely by the absence of a Q-loop. The significant difference in the position of the general acid loop among classical PTPs, LMW PTPs, and VH1-related DSPs undoubtedly contributes as well.

(3) The presence of phosphotransferase activity in some phosphatases, but not others, may have biological consequences. It may not be coincidental that some proteins known to be associated with cancer, such as VH1-related DSPs and LMW PTPs, and, recently, VHZ,³⁶ reveal a high level of phosphotransferase ability. Whether this process is random and nonspecific, or transphosphorylation is selective for some protein target, remains to be discovered. However, because VHZ has a stringent phosphotyrosine specificity because of its deep and narrow active site, we can conclude that its transphosphorylation target would likely be limited to tyrosine protein sites, or to small molecule nucleophile acceptors capable of entering the active site.

ASSOCIATED CONTENT

Supporting Information

Table of ionization constants associated with catalytically relevant residues, plot of partial extinction coefficients for *p*-nitrophenol versus pH, derivation of equations for PTP-catalyzed reactions in the presence of alternative nucleophiles, a kinetic model including two coexisting substrate binding

modes, and a sequence alignment of VHZ, SsoPTP, and Tk-PTP. This material is available free of charge via the Internet at <http://pubs.acs.org>.

AUTHOR INFORMATION

Corresponding Author

*E-mail: alvan.hengge@usu.edu. Phone: (435) 797-3442. Fax: (435) 797-3390.

Funding

This work was supported by National Institutes of Health Grant GM47297 (A.C.H.).

Notes

The authors declare no competing financial interest.

ACKNOWLEDGMENTS

We thank Dr. Edwin Antony for use of his stopped-flow spectrophotometer.

ABBREVIATIONS

KIE, kinetic isotope effect; VHR, Vaccinia H1-related protein member R; LDP, low-molecular weight dual-specificity phosphatase; VHZ, Vaccinia H1-related protein member Z; YopH, *Yersinia* outer protein type H; SsoPTP, *S. solfataricus* protein tyrosine phosphatase; DSP, dual-specificity phosphatase; *p*NPP, *p*-nitrophenyl phosphate; IPTG, isopropyl β -D-1-thiogalactopyranoside; TEV, tobacco etch virus; PDB, Protein Data Bank.

REFERENCES

- (1) Tonks, N. K. (2006) Protein tyrosine phosphatases: From genes, to function, to disease. *Nat. Rev. Mol. Cell Biol.* 7, 833–846.
- (2) Zhang, Z. Y., Wang, Y., and Dixon, J. E. (1994) Dissecting the catalytic mechanism of protein-tyrosine phosphatases. *Proc. Natl. Acad. Sci. U.S.A.* 91, 1624–1627.
- (3) Zhang, Z. Y., Malachowski, W. P., Van Etten, R. L., and Dixon, J. E. (1994) Nature of the rate-determining steps of the reaction catalyzed by the *Yersinia* protein-tyrosine phosphatase. *J. Biol. Chem.* 269, 8140–8145.
- (4) Wang, W. Q., Sun, J. P., and Zhang, Z. Y. (2003) An overview of the protein tyrosine phosphatase superfamily. *Curr. Top. Med. Chem.* 3, 739–748.
- (5) Patterson, K. I., Brummer, T., O'Brien, P. M., and Daly, R. J. (2009) Dual-specificity phosphatases: Critical regulators with diverse cellular targets. *Biochem. J.* 418, 475–489.
- (6) Zhao, Y., Wu, L., Noh, S. J., Guan, K. L., and Zhang, Z. Y. (1998) Altering the nucleophile specificity of a protein-tyrosine phosphatase-catalyzed reaction. Probing the function of the invariant glutamine residues. *J. Biol. Chem.* 273, 5484–5492.
- (7) Paoli, P., Modesti, A., Magherini, F., Gamberi, T., Caselli, A., Manao, G., Raugei, G., Camici, G., and Ramponi, G. (2007) Site-directed mutagenesis of two aromatic residues lining the active site pocket of the yeast Ltp1. *Biochim. Biophys. Acta* 1770, 753–762.
- (8) Kuznetsov, V. I., Hengge, A. C., and Johnson, S. J. (2012) New Aspects of the Phosphatase VHZ Revealed by a High-Resolution Structure with Vanadate and Substrate Screening. *Biochemistry* 51, 9869–9879.
- (9) Chu, H. M., and Wang, A. H. (2007) Enzyme-substrate interactions revealed by the crystal structures of the archaeal *Sulfolobus* PTP-fold phosphatase and its phosphopeptide complexes. *Proteins* 66, 996–1003.
- (10) Brandão, T. A. S., Hengge, A. C., and Johnson, S. J. (2010) Insights into the Reaction of Protein-tyrosine Phosphatase 1B. *J. Biol. Chem.* 285, 15874–15883.
- (11) Brandao, T. A., Robinson, H., Johnson, S. J., and Hengge, A. C. (2009) Impaired acid catalysis by mutation of a protein loop hinge

residue in a YopH mutant revealed by crystal structures. *J. Am. Chem. Soc.* 131, 778–786.

(12) Bourne, N., and Williams, A. (1984) Effective charge on oxygen in phosphoryl group transfer from an oxygen donor. *J. Org. Chem.* 49, 1200–1204.

(13) Hengge, A. C. (2002) Isotope effects in the study of phosphoryl and sulfuryl transfer reactions. *Acc. Chem. Res.* 35, 105–112.

(14) Hengge, A. C., and Cleland, W. W. (1990) Direct measurement of transition-state bond cleavage in hydrolysis of phosphate esters of p-nitrophenol. *J. Am. Chem. Soc.* 112 (20), 7421–7422.

(15) Trott, O., and Olson, A. J. (2010) AutoDock Vina: Improving the speed and accuracy of docking with a new scoring function, efficient optimization, and multithreading. *J. Comput. Chem.* 31, 455–461.

(16) Seeliger, D., and de Groot, B. L. (2010) Ligand docking and binding site analysis with PyMOL and Autodock/Vina. *J. Comput.-Aided Mol. Des.* 24, 417–422.

(17) Rarey, M., Kramer, B., and Lengauer, T. (1995) Time-efficient docking of flexible ligands into active sites of proteins. *Proc. Int. Conf. Intell. Syst. Mol. Biol.*, 3rd 3, 300–308.

(18) Fuhrmann, J., Rurainski, A., Lenhof, H. P., and Neumann, D. (2010) A new Lamarckian genetic algorithm for flexible ligand-receptor docking. *J. Comput. Chem.* 31, 1911–1918.

(19) Hengge, A. C., Denu, J. M., and Dixon, J. E. (1996) Transition-state structures for the native dual-specific phosphatase VHR and D92N and S131A mutants. Contributions to the driving force for catalysis. *Biochemistry* 35, 7084–7092.

(20) Alonso, A., Burkhalter, S., Sasin, J., Tautz, L., Bogetz, J., Huynh, H., Bremer, M. C., Holsinger, L. J., Godzik, A., and Mustelin, T. (2004) The minimal essential core of a cysteine-based protein-tyrosine phosphatase revealed by a novel 16-kDa VH1-like phosphatase, VHZ. *J. Biol. Chem.* 279, 35768–35774.

(21) Takagaki, K., Satoh, T., Tanuma, N., Masuda, K., Takekawa, M., Shima, H., and Kikuchi, K. (2004) Characterization of a novel low-molecular-mass dual-specificity phosphatase-3 (LDP-3) that enhances activation of JNK and p38. *Biochem. J.* 383, 447–455.

(22) Wu, Q., Li, Y., Gu, S., Li, N., Zheng, D., Li, D., Zheng, Z., Ji, C., Xie, Y., and Mao, Y. (2004) Molecular cloning and characterization of a novel dual-specificity phosphatase 23 gene from human fetal brain. *Int. J. Biochem. Cell Biol.* 36, 1542–1553.

(23) Denu, J. M., Lohse, D. L., Vijayalakshmi, J., Saper, M. A., and Dixon, J. E. (1996) Visualization of intermediate and transition-state structures in protein-tyrosine phosphatase catalysis. *Proc. Natl. Acad. Sci. U.S.A.* 93, 2493–2498.

(24) Flint, A. J., Tiganis, T., Barford, D., and Tonks, N. K. (1997) Development of “substrate-trapping” mutants to identify physiological substrates of protein tyrosine phosphatases. *Proc. Natl. Acad. Sci. U.S.A.* 94, 1680–1685.

(25) Zhang, Z. Y., Wu, L., and Chen, L. (1995) Transition state and rate-limiting step of the reaction catalyzed by the human dual-specificity phosphatase, VHR. *Biochemistry* 34, 16088–16096.

(26) Hengge, A. C., Sowa, G. A., Wu, L., and Zhang, Z. Y. (1995) Nature of the transition state of the protein-tyrosine phosphatase-catalyzed reaction. *Biochemistry* 34, 13982–13987.

(27) Brandao, T. A., Johnson, S. J., and Hengge, A. C. (2012) The molecular details of WPD-loop movement differ in the protein-tyrosine phosphatases YopH and PTP1B. *Arch. Biochem. Biophys.* 525, 53–59.

(28) Hengge, A. C., Zhao, Y., Wu, L., and Zhang, Z. Y. (1997) Examination of the transition state of the low-molecular mass small tyrosine phosphatase I. Comparisons with other protein phosphatases. *Biochemistry* 36, 7928–7936.

(29) Pannifer, A. D., Flint, A. J., Tonks, N. K., and Barford, D. (1998) Visualization of the cysteinyl-phosphate intermediate of a protein-tyrosine phosphatase by X-ray crystallography. *J. Biol. Chem.* 273, 10454–10462.

(30) Dick, C. F., Dos-Santos, A. L. A., and Meyer-Fernandes, J. R. (2011) Inorganic Phosphate as an Important Regulator of Phosphatases. *Enzyme Res.* 2011, 1–7.

(31) Marshall, W. J., and Bangert, S. K. (2008) *Clinical Biochemistry: Metabolic and Clinical Aspects*, 2nd ed., Elsevier, Amsterdam.

(32) Chang, M. W., Ayeni, C., Breuer, S., and Torbett, B. E. (2010) Virtual screening for HIV protease inhibitors: A comparison of AutoDock 4 and Vina. *PLoS One* 5, e11955.

(33) Sousa, S. F., Fernandes, P. A., and Ramos, M. J. (2006) Protein-ligand docking: Current status and future challenges. *Proteins* 65, 15–26.

(34) Jeon, S. J., Fujiwara, S., Takagi, M., Tanaka, T., and Imanaka, T. (2002) Tk-PTP, protein tyrosine/serine phosphatase from hyperthermophilic archaeon *Thermococcus kodakaraensis* KOD1: Enzymatic characteristics and identification of its substrate proteins. *Biochem. Biophys. Res. Commun.* 295, 508–514.

(35) Luechapanichkul, R., Chen, X., Taha, H. A., Vyas, S., Guan, X., Freitas, M. A., Hadad, C. M., and Pei, D. (2013) Specificity profiling of dual specificity phosphatase vaccinia VH1-related (VHR) reveals two distinct substrate binding modes. *J. Biol. Chem.* 288, 6498–6510.

(36) Tang, J. P., Tan, C. P., Li, J., Siddique, M. M., Guo, K., Chan, S. W., Park, J. E., Tay, W. N., Huang, Z. Y., Li, W. C., Chen, J., and Zeng, Q. (2010) VHZ is a novel centrosomal phosphatase associated with cell growth and human primary cancers. *Mol. Cancer*, 128.